

See discussions, stats, and author profiles for this publication at: <https://www.researchgate.net/publication/256248126>

# Interplay between Hydrogen Bonding and Molecule–Substrate Interactions in the Case of Terephthalic Acid Molecules on Cu(001) Surfaces

**DATASET** in THE JOURNAL OF PHYSICAL CHEMISTRY C · JANUARY 2013

Impact Factor: 4.77 · DOI: 10.1021/jp305455v

CITATIONS

8

READS

62

9 AUTHORS, INCLUDING:



**Javier Daniel Fuhr**

National Scientific and Technical Research Co...

27 PUBLICATIONS 228 CITATIONS

SEE PROFILE



**Albano Cossaro**

Italian National Research Council

75 PUBLICATIONS 1,554 CITATIONS

SEE PROFILE



**J. Esteban Gayone**

Centro Atómico Bariloche

57 PUBLICATIONS 817 CITATIONS

SEE PROFILE



**Hugo Ascolani**

Centro Atómico Bariloche, Comisión Nacional ...

49 PUBLICATIONS 488 CITATIONS

SEE PROFILE

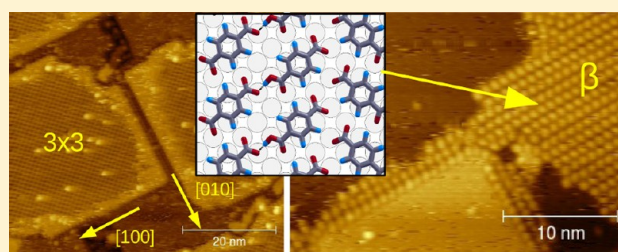
# Interplay between Hydrogen Bonding and Molecule–Substrate Interactions in the Case of Terephthalic Acid Molecules on Cu(001) Surfaces

J. D. Fuhr,<sup>\*,†</sup> A. Carrera,<sup>†</sup> N. Murillo-Quirós,<sup>†</sup> L. J. Cristina,<sup>†</sup> A. Cossaro,<sup>‡</sup> A. Verdini,<sup>‡</sup> L. Floreano,<sup>‡</sup> J. E. Gayone,<sup>†</sup> and H. Ascolani<sup>\*,†</sup>

<sup>†</sup>Centro Atómico Bariloche, Comisión Nacional de Energía Atómica, and Consejo Nacional de Investigaciones Científicas y Técnicas, Avda. E. Bustillo 9500, R8402AGP, Bariloche, Argentina

<sup>‡</sup>CNR-IOM, Laboratorio TASC, Basovizza SS14 km 163.5, I-34149 Trieste, Italy

**ABSTRACT:** The adsorption and self-assembling properties of terephthalic acid (TPA) molecules deposited on Cu(001) at room temperature have been systematically studied with both experimental and theoretical tools. The system forms two phases at room temperature: the metastable  $\beta$ -phase and the stable  $(3 \times 3)$  one. In the case of the  $\beta$  phase, low-energy electron diffraction and scanning tunneling microscopy (STM) results indicate that it has a  $(9\sqrt{2} \times 2\sqrt{2}) R45^\circ$  unit cell with exactly the same molecular coverage as the  $(3 \times 3)$  phase. In addition, the high-resolution X-ray photoelectron-spectroscopy spectra of the O 1s core level indicate that the irreversible  $\beta \rightarrow (3 \times 3)$  transition involves the following two processes: (i) deprotonation of the complete carboxyl groups remaining in the metastable phase and (ii) eventual rearrangement of the molecules into the  $3 \times 3$  configuration. We explored possible molecular configurations for the  $\beta$  phase with different degree of deprotonation (including structures with Cu adatoms) by means of density functional theory calculations. Our theoretical results indicate the formation of strong bonds between the O atoms in carboxylates and the Cu atoms of the surface, which causes a bending of the molecules and a buckling of the first Cu layer. In the  $(3 \times 3)$  phases, we show that the bending produces observable effects in the molecular STM images. Moreover, the strong interaction between the carboxylates and the Cu atoms at the step edges drives the reorientation of the surface steps along the  $\langle 100 \rangle$  crystallographic directions.



## INTRODUCTION

Engineering of supramolecular structures grown by spontaneous self-assembling on metallic surfaces is important in nanotechnology.<sup>1</sup> Molecules with well-defined shapes and multiple sites that engage in strong directional interactions are now widely used to build new ordered materials on surfaces.<sup>2,3</sup> In this article we consider the ordered phases formed by terephthalic acid (TPA) molecules on Cu(001) surfaces at room temperature (RT) as a model system to investigate the subtle energetical balance between molecule–substrate interactions and intermolecular interactions. A deep understanding of this balance is important to predict the physical–chemical properties of two-dimensional (2D) supramolecular structures grown on surfaces.<sup>4</sup>

TPA is the simplest case of rodlike polybenzene dicarboxylic acids, a family of molecules that has been widely used as linkers to build interesting 2D supramolecular structures.<sup>5</sup> The versatility of these molecules is strongly related to the carboxyl groups (RCOOH). It is well-established that the RCOOH group usually remains intact upon adsorption on low-reactivity surfaces, such as Au(111)<sup>6,7</sup> and highly oriented pyrolytic graphite (HOPG)<sup>8</sup> surfaces. The group can lose the proton when deposited on more reactive substrates, for example,

Cu<sup>9–14</sup> or Ag<sup>15,16</sup> surfaces. In the first case, the neutral TPA molecules form highly ordered supramolecular structures governed by strong [O–H...O] hydrogen bonds.<sup>6</sup> In the second case, deprotonation of carboxyl groups opens the route to metal–organic complexes, offering a variety of possibilities to produce 2D magnetic networks based on Fe<sup>17–21</sup> and Mn<sup>22</sup> with exciting properties.

Although the TPA/Cu(001) system has been widely applied to grow 2D supramolecular structures, there are important issues concerning the pure system that are still open. The phases formed by TPA molecules on the Cu(001) surface have been previously investigated by Stepanow et al.<sup>12</sup> by means of scanning tunneling microscopy (STM), X-ray photoelectron spectroscopy (XPS), and near-edge X-ray absorption fine structure (NEXAFS). Three distinct ordered phases evolving with increasing temperature were observed. Deposition on samples kept at temperatures below 230 K produced the  $\alpha$  phase, which, according to the reported STM image, consists of thin and long molecular ribbons oriented along specific

Received: June 4, 2012

Revised: December 20, 2012

Published: December 27, 2012



directions of the substrate. Both the anisotropic growth of the islands as well as the C 1s and O 1s XPS spectra taken for this phase are consistent with neutral TPA molecules interacting through [O–H...O] hydrogen bonds. Increasing the sample temperature to about 273 K produced transformation of the low-temperature phase into a metastable ordered phase called  $\beta$ . It was speculated that this phase contains both complete and deprotonated carboxyl groups in equal amounts. At RT, a mixture of the  $\beta$  and  $\gamma$  phases was observed. The  $\gamma$  phase has a  $3 \times 3$  periodicity and is composed of TPA molecules with the two carboxyl groups deprotonated (terephthalates).<sup>23</sup> Finally, a pure  $(3 \times 3)$  phase was obtained after a mild annealing of the sample to 400 K.

Figure 1 shows a scheme of the structural model proposed for  $(3 \times 3)$  phase. The O atoms are expected to form strong

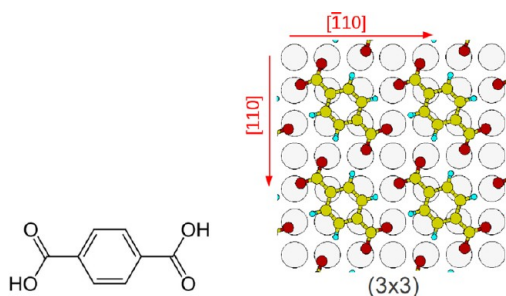


**Figure 1.** (Left) Scheme of the TPA molecule. (Right) Structural model for the  $(3 \times 3)$  phase of deprotonated TPA molecules on Cu(001). Yellow, light blue, and red circles represent C, H and O atoms of deprotonated TPA molecules, respectively. Large open circles represent the Cu atoms of the top surface layer.

Cu–O bonds and also weak hydrogen bonds with the H atoms of the benzene ring. It is now well recognized that [C–H...O] hydrogen bonds play a fundamental role in determining the packing of organic molecules in the solid state.<sup>24</sup> Similarly, [C–H...O] hydrogen bonds are expected to be an important factor for the stabilization of two-dimensional molecular structures on surfaces. In the particular case of the  $(3 \times 3)$  structure, the formation of [C–H...O] bonds (eight bonds per molecule) has been regarded as the main driving force for the formation of the phase.<sup>12</sup> However, Ge et al.<sup>23</sup> did not observe any evidence for this type of H bonding in their high-resolution electron energy-loss spectroscopy (HREELS) spectra and, hence, suggested that TPA islanding may be due to surface-mediated attractive interactions.<sup>4</sup> As the atomic structure of the  $(3 \times 3)$  phase has not been quantitatively investigated either experimentally or theoretically, the relative importance of these effects is not known.

The  $\beta$  phase is also interesting from the structural point of view since, in addition to the weak [C–H...O] bonds found in the  $(3 \times 3)$  phase, it would involve strong [O–H...O] bonds. However, there is almost no quantitative information on this metastable phase in the literature so far. A quantitative knowledge of the structure would help to gain more understanding of the deprotonation process of TPA molecules on the Cu(001) surface.

In this work we performed a systematic and quantitative characterization of the atomic and electronic structures of the  $(3 \times 3)$  and  $\beta$  phases by combining different experimental techniques, namely, low-energy electron diffraction (LEED), STM, and high-resolution XPS (HR-XPS), with van der Waals density functional theory (DFT) calculations. Our results

allowed us to perform a detailed analysis of the competition between substrate/molecule interactions and hydrogen-bond interactions taking place in the TPA/Cu(001) system.

## METHODS

**Experimental Details.** Two independent ultrahigh vacuum systems were used to perform the experiments involved in this work. The LEED and STM experiments were carried out at Bariloche in an ultrahigh vacuum system from Omicron Nanotechnology. The HR-XPS experiments were carried out at the Aloisa beamline<sup>25,26</sup> of the Elettra synchrotron, at Trieste.

The base pressures in both chambers were in the low  $10^{-10}$  mbar range. The Cu(001) surfaces were prepared by cycles of sputtering with Ar at 1.5 keV and annealing at 770 K. The TPA molecules (Sigma–Aldrich, 98% purity) were used as received. In all cases analyzed in this work, the TPA/Cu(001) samples were prepared by dosing TPA molecules (submonolayer range) on the substrate at RT. The molecules were evaporated from a resistivity heated BN crucible at a rate of about 0.1 monolayer (ML) per minute. We define 1 ML as the surface coverage corresponding to the  $(3 \times 3)$  phase, that is, a molecular coverage of 1 TPA molecule per 9 Cu atoms in the top surface layer. In Aloisa we checked the formation of the  $(3 \times 3)$  phase as well as the quality of the clean Cu(001) surface by reflection high-energy electron diffraction (RHEED).

All the reported STM images were taken at RT (unless otherwise stated) with W tips. Negative sample bias voltages correspond to occupied-state images. The thermal drift was compensated during the measurements by applying the facility provided by the MATRIX software used to control the STM.

The HR-XPS data were obtained by use of a p-polarized X-ray beam at grazing incidence (about  $4^\circ$ ). The spectra, taken with a photon energy of 655 eV, were measured in normal emission by means of a hemispherical electron analyzer with angular acceptance of  $2^\circ$  and an overall energy resolution of 300 meV. Four energy windows, centered on the regions of the Fermi edge and the Cu 3p, C 1s, and O 1s core levels, were typically acquired by means of a 2D delay-line detector.<sup>27</sup>

**Theoretical Details.** The DFT calculations were performed using the Quantum-ESPRESSO package,<sup>28</sup> which is an implementation of the plane-wave with ultrasoft pseudopotentials approach. The exchange–correlation effects were treated by use of the second version of van der Waals density functional (vdW-DF)<sup>29</sup> with improved exchange.<sup>30</sup> For the surface calculations we have used the slab method, with four Cu layers representing the surface and an equivalent vacuum size of seven layers. For all the calculations, we fixed the two lower layers while all other atoms were allowed to relax. We used a wave function/charge cutoff of 30/300 Ry, and Brillouin integrations were done with grids of  $15 \times 15 \times 1$ ,  $5 \times 5 \times 1$ , and  $3 \times 3 \times 1$  k-points for the unit cell, the  $3 \times 3$  supercell, and the  $5 \times 5$  supercell, respectively.

For a given configuration corresponding to  $N$  molecules adsorbed on the surface, the mean adsorption energy per molecule is calculated by

$$E_{\text{ads}}(\text{TPA}) = - \left[ \frac{E_{\text{total}} - E_{\text{surface}} - N_{\text{H}} E_{\text{ads}}(\text{H})}{N} - E_{\text{TPA}} \right] \quad (1)$$

where  $E_{\text{total}}$  is the total energy of the system with the adsorbed molecules;  $E_{\text{surface}}$  is the total energy of a clean surface with the



same area;  $N_{\text{H}}$  is the number of dissociated H atoms, with  $E_{\text{ads}}(\text{H}) = 0.18$  eV its corresponding adsorption energy on the Cu(001) surface; and  $E_{\text{TPA}}$  is the total energy of an isolated TPA molecule.

In all the calculations we have applied the dipole correction, which takes into account the possible dipoles that can appear on the surfaces.<sup>31</sup> As the two surfaces of the slab are not equal, the lower one clean while the upper one has adsorbed molecules, the difference in the surfaces dipoles is compensated in the middle of the vacuum by an artificial jump in the potential. The simulated STM images were calculated within the Tersoff–Hamann approximation.<sup>32</sup>

## RESULTS

### Experimental Results. Low-Energy Electron Diffraction.

Figure 2a,b shows two LEED patterns measured with 37 and 51

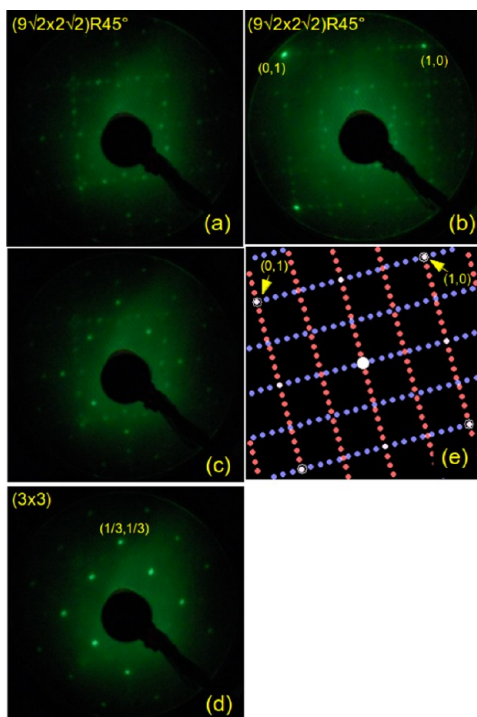


**Figure 2.** (a, b) Experimental LEED patterns representative of fresh TPA/Cu(001) surfaces prepared at RT; the corresponding electron energies are (a) 37 and (b) 51 eV. The  $(1 \times 1)$  spots are outside the screen in pattern a, while they are clearly visible in pattern b. (c, d) Transformation of pattern a into a  $(3 \times 3)$  one; they were recorded after (c) 9 and (d) 30 min of having measured the initial pattern. The observed phase transition is induced by the primary electron beam of the LEED (see text for details). (e) Simulated LEED pattern<sup>33</sup> for a  $(9\sqrt{2} \times 2\sqrt{2})$   $R45^\circ$  unit cell; the blue and red spots correspond to patterns of the two inequivalent domains of the superstructure.

eV, respectively, which are representative of freshly prepared TPA/Cu(001) surfaces. These patterns, which have not been previously reported in the literature, were observed to be highly unstable under the effect of the primary electron beam of the LEED. The effect is illustrated by the series of patterns in Figure 2a,c,d. As seen in these images, the initial LEED pattern completely transform into a  $(3 \times 3)$  one within a period of 30 min. We note, however, that this effect is not observed when the e-beam is turned off; in this case the lifetime of the initial pattern was observed to be several hours. It should be noted

that the initial pattern in Figure 2a also contains weak  $(3 \times 3)$  spots.

In ref 12, it was shown that deposition of TPA on Cu(001) at RT produces a surface where the  $(3 \times 3)$  phase coexists with the metastable  $\beta$  one. Therefore, the LEED patterns shown in Figure 2a,b should correspond to a mixture of these phases. What it is unexpected, however, is the fact that the pattern of the metastable  $\beta$  phase systematically turned out to be highly dominant in fresh samples.

From a detailed analysis of the patterns in Figure 2a,b, we concluded that they correspond to a  $(9\sqrt{2} \times 2\sqrt{2})$   $R45^\circ$  superstructure (denoted  $9\sqrt{2}$  hereafter). This fact can be corroborated by comparing the experimental patterns with the simulated one in Figure 2e. The spots that cannot be explained by the  $9\sqrt{2}$  superstructure correspond to the  $(3 \times 3)$  phase.

**Scanning Tunneling Microscopy.** Figure 3a shows an STM image with molecular resolution where two inequivalent rotated

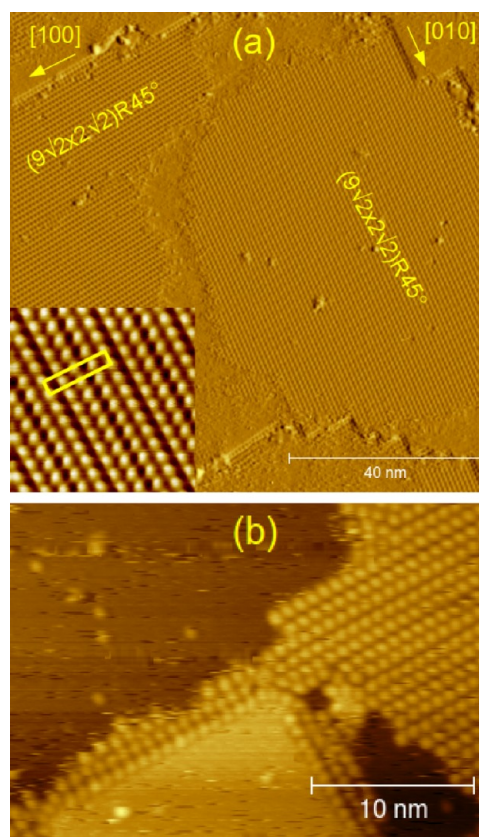


**Figure 3.** (a) Occupied-state STM image (gradient mode) where two  $90^\circ$  rotated domains of the  $9\sqrt{2}$  phase are seen. Tunneling conditions:  $-2$  V/10 pA. (Inset) Zoomed area ( $100 \times 100 \text{ \AA}^2$ ) of the domain on the right; a yellow rectangle is superimposed on the image, indicating the unit cell of the superstructure. (b) STM image taken under the same tunneling conditions as in panel a but with the sample cooled to around 200 K.

domains of the  $\beta$  phase can be clearly seen. The image was taken on a fresh sample where no further bombarding with the LEED electron beam was done. Remarkably, this area of the surface was scanned along several hours at RT and we did not detect any transformation to the  $(3 \times 3)$  phase. In agreement with the LEED results, the STM experiments show that the  $\beta$  phase covers most of the surface, even when it was always found coexisting with  $(3 \times 3)$  islands.

In order to determine the unit cell of the  $\beta$  phase, we used STM images where domains of the  $(3 \times 3)$  phase are also seen. These kind of images allowed us to perform a precise correction of the remaining distortions of the images, since we could take the  $(3 \times 3)$  superstructure as a reference. We determined that the unit cell of the  $\beta$  phase is rectangular ( $\alpha = 90^\circ \pm 1^\circ$ ) with sides of  $7.3 \pm 0.5$  and  $34 \pm 2$  Å. These values agree very well with the corresponding exact values of the  $9\sqrt{2}$  unit cell (7.22 and 32.50 Å), giving support to the conclusions derived from the LEED experiments. We note that neither the STM images nor the LEED pattern of the  $\beta$  phase are consistent with the unit cell proposed by Stepanow et al.<sup>12</sup>

$$\begin{pmatrix} 2 & -2 \\ 4 & 5 \end{pmatrix}$$

Finally, as we shall show in the next section (see Figure 11), there are four molecules in the unit cell, and therefore, the coverage of the phase is 1 TPA molecule per 9 Cu atoms of the first substrate layer. Notably, the  $9\sqrt{2}$  phase has exactly the same molecular coverage as the  $(3 \times 3)$  phase (from this point we will refer to " $\beta$  phase" as " $9\sqrt{2}$  phase")

The STM image of Figure 3a also illustrates about another interesting effect systematically observed in our images: the straightening of monatomic surface steps along the  $\langle 100 \rangle$  crystallographic directions induced by the adsorption of the TPA molecules for submonolayer coverages. This is in contrast to the fact that for Cu(001) surfaces the energetically more stable steps are those aligned along  $\langle 110 \rangle$  directions. We note that a similar effect was observed for submonolayer coverage of tetrafluorotetracyanoquinodimethane (F-TCNQ) adsorbed on Cu(001) surfaces.<sup>34</sup> The reorientation effect is illustrated with more detail in Figure 3b, which was measured after cooling of the sample to 200 K in order to reduce the mobility of the molecules. This image shows a small monatomic terrace with squarelike shape close to an island of molecules in the  $9\sqrt{2}$  phase. The monatomic steps are decorated at the lower edge by a few lines of molecules arranged with a similar orientation as that observed in the  $9\sqrt{2}$  island, indicating that the interaction of the TPA molecules with the Cu atoms at the steps is responsible for this effect. These observations would be related to the origin of the multistep squared-shape terraces recently reported by Tait et al.<sup>35</sup> for a saturated monolayer of TPA on Cu(001).

In addition, Figure 4 shows a TPA/Cu(001) surface after annealing of the sample to 400 K for a few minutes. The resulting surface is composed of monatomic squared-shape terraces with their delimiting steps aligned along the  $\langle 100 \rangle$  crystallographic directions of the substrate; the average size of the terraces is around  $300 \times 300$  Å<sup>2</sup>. Islands of the  $(3 \times 3)$  phase cover the upper surface of the square terraces. Also, it can be seen in this image that the straight segments of the steps are decorated by molecules. We therefore conclude that the typical annealing used to obtain the  $(3 \times 3)$  phase in fact produces a surface with a high density of surface steps oriented along the  $\langle 100 \rangle$  crystallographic directions. The observed drastic change of the surface morphology with annealing at 400 K is probably related to the thermal dependence of the diffusion of the Cu atoms at the steps, which is a thermally activated process. Kinks are known to reach a high mobility at 360 K in Cu(001) surfaces.<sup>36</sup>

**X-ray Photoelectron Spectroscopy.** As discussed above, the  $9\sqrt{2}$  phase covers most of the surface when submonolayer

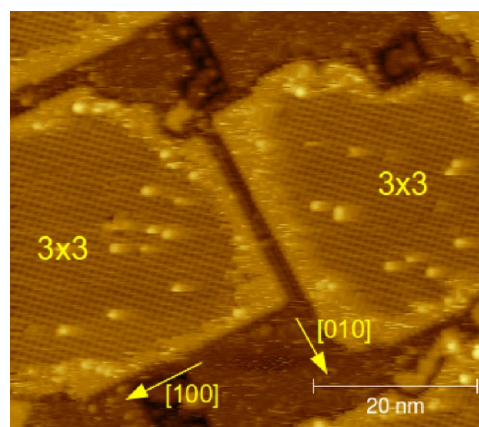


**Figure 4.** Occupied-state STM image of the TPA/Cu(001) surface after annealing of the sample to 400 K. Tunneling conditions:  $-2$  V/10 pA.

amounts of TPA molecules are adsorbed on Cu(001) at RT. This situation was observed to be stable for a few hours, provided the surface was not irradiated with the primary electron gun of the LEED. These properties of the  $9\sqrt{2}$  phase allowed us to characterize it by means of HR-XPS. Figure 5

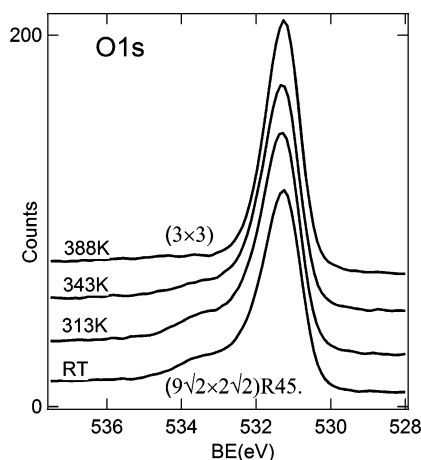


**Figure 5.** Series of O 1s spectra corresponding to a submonolayer amount of TPA adsorbed on Cu(001) at RT obtained as a function of the annealing temperature of the prepared sample. The lower and upper spectra are representative of the  $9\sqrt{2}$  and  $(3 \times 3)$  phases, respectively.

shows the O 1s XPS spectrum obtained after adsorption of the TPA at RT (lower one), together with three spectra measured after annealing of the prepared sample for 5 min at different temperatures. The four spectra were normalized to the intensity of the corresponding Cu 3p peak, and therefore, their relative intensities are comparable. To calibrate the binding energy of each spectrum, we considered both the Fermi level edge and the Cu 3p peak.

Therefore, the lower spectrum in Figure 5 is representative of the  $9\sqrt{2}$  phase. The upper spectrum, in turn, corresponds to the  $(3 \times 3)$  phase of the system, as checked by RHEED. The spectrum of the  $9\sqrt{2}$  phase presents, apart from the prominent peak centered around 531 eV that corresponds to carboxylates, a clear shoulder toward higher binding energies (which extends up to about 534 eV), which strongly suggests the existence of complete carboxyl groups, as proposed by Stepanow et al.<sup>12</sup>



In Figure 6 we show a component analysis of the O 1s spectrum representative of the  $9\sqrt{2}$  phase. We used three

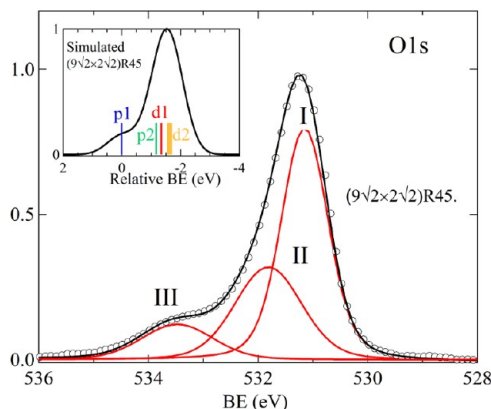


**Figure 6.** Analysis of O 1s spectrum corresponding to the  $9\sqrt{2}$  phase. (O) Experimental data; (—) result of the fitting. The spectrum is normalized to their corresponding maxima. (Inset) Simulated spectrum as explained in the text.

Voigt functions and a Shirley-type background to fit the experimental spectrum. The optimized parameter values obtained for components I, II, and III are the following: Gaussian widths were 0.86, 1.3, and 1.4 eV, respectively; the three Lorentzian widths were fixed to 0.25 eV. Binding energies were 531.1, 531.7, and 533.3 eV, respectively. Finally, the resulting relative peak areas for components I, II, and III turned out to be 56%, 31%, and 13%, respectively.

The binding-energy values obtained for components I and III agree very well with the previously reported values for O atoms in carboxylates bonded to Cu surfaces and for the OH part of the RCOOH groups, respectively.<sup>9,12–14,19,37</sup> Thus, component III confirms that the  $9\sqrt{2}$  phase comprises carboxyl groups. Regarding component II, we note that it is shifted by 1.6 eV from component III. We recall that the shift between the O 1s peaks corresponding to OH and C=O groups is 1.4 eV for TPA molecules in bulk and 2.05 eV for TPA in gas phase.<sup>38,39</sup> Thus, component II should contain the contribution of the C=O groups, although it could also include the contributions of other chemically inequivalent O atoms of the  $9\sqrt{2}$  structure, as suggested by the simulated O 1s spectrum shown in the inset. We shall discuss the simulated spectrum in the next section.

The O 1s spectra in Figure 5 show the irreversible transition from partially protonated  $9\sqrt{2}$  phase to fully deprotonated ( $3 \times 3$ ) phase induced by temperature. Notice that annealing the sample to 313 K does not produce any noticeable change in the O 1s peak, while in turn, annealing to 343 K produces a clear reduction of the shoulder and, at the same time, an increment of the main-peak intensity. Notably, a quantitative analysis of the spectra indicates that the total area under the normalized O 1s spectra remains constant during the transition, as expected for a transition between two phases with the same molecular coverage. We therefore conclude that the transition involves the following two processes: (i) deprotonation of the carboxyl groups remaining in the  $9\sqrt{2}$  phase and (ii) eventual rearrangement of the molecules into the ( $3 \times 3$ ) configuration.

**Density Functional Theory Calculations.** In order to gain more understanding of the physical–chemical processes taking place at the molecule/substrate interfaces formed in this system, we carried out a thorough theoretical study of the adsorption of TPA molecules on the Cu(001) surface.

We first studied a single TPA molecule in a  $5 \times 5$  supercell, which corresponds to the system with the lowest molecule–molecule interaction of our calculations. We considered both neutral molecules and molecules with the two carboxyl groups deprotonated (also called totally deprotonated TPA molecules in this article), and in both cases we found two local minimum-energy configurations with the center of the benzene in a hollow site and the molecule oriented in [100] and [110] surface directions (see Figure 7). In both cases, neutral and

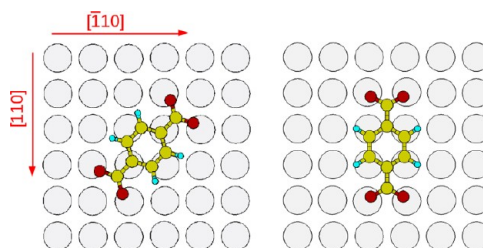


**Figure 7.** Two adsorption geometries for isolated deprotonated TPA molecules on Cu(001) from DFT calculations. Left: molecule oriented in the [100] direction. Right: molecule oriented in the [110] direction.

deprotonated molecule, the minimum energy corresponds to the molecule aligned in the [100] direction (Figure 7, left panel) with adsorption energies of 1.80 and 2.08 eV, respectively. The gain in energy by dissociation of the molecule, with the H remaining on the surface (see eq 1), is then 0.28 eV. On the other hand, the configurations with the molecule aligned in the [110] direction have lower adsorption energies by 0.20 eV.

Notably, our calculations indicate that the molecule/substrate interaction is strong in both neutral and deprotonated molecule. In the lowest-energy configuration, the deprotonated molecule is bent with a difference of 0.26 Å between the height of the benzene ring and the O atoms. The adsorption of the molecule produces also a significant displacement of the Cu surface atoms out from their equilibrium positions, resulting in a corrugation of the top Cu layer of 0.16 Å. In the case of the protonated molecule, the optimized configuration presents the carboxyl groups rotated with the oxygen in the OH group moving upward by 0.35 Å with respect to the C atom in the group, and the other O moving downward by 0.15 Å. This means that even in the case of the protonated TPA molecule there is a rather strong O–Cu bonding.

Having studied the case of isolated molecules, the next step is to study the energetics and the properties of the ( $3 \times 3$ ) phase. In a  $3 \times 3$  supercell there is not enough space for the molecule in the [110] orientation, and therefore the molecular configuration must be the one shown in Figure 1. In this superstructure, the optimized adsorption geometry of the molecule is very similar to the isolated one, with a bending of 0.26 Å between the height of the benzene and the O atoms and a corrugation in the last Cu layer of 0.16 Å (see Figure 8). The

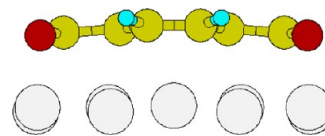


**Figure 8.** Side view of the lowest-energy adsorption geometry obtained for the ( $3 \times 3$ ) phase of TPA molecules on Cu(001).

calculated adsorption energy per molecule is 2.28 eV, indicating a stabilization of the ordered phase with a gain of 0.20 eV/molecule. This energy gain has contributions from direct molecule interactions, mainly by formation of [C–H...O] bonds, and from substrate-mediated interactions. As pointed out by Tseng et al.,<sup>4</sup> the molecule-induced surface corrugation can cause an attractive intermolecular interaction.

From the relaxed structure of this ( $3 \times 3$ ) phase, we simulated STM images for positive and negative bias voltage  $V_b$ . Figure 9 compares the simulated images obtained for  $V_b = \pm 1.6$

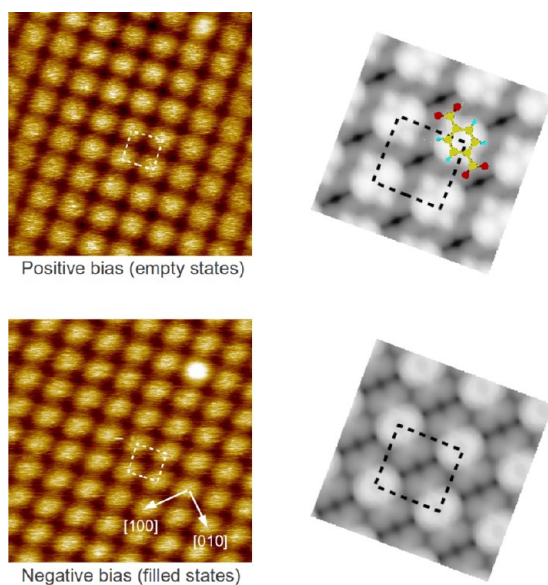


**Figure 9.** (Left) Experimental and (right) simulated STM images of the ( $3 \times 3$ ) phase for positive and negative sample bias: (top) +1.6 V; (bottom) –1.6 V. The tunneling current and the size values corresponding to the experimental images are 100 pA and  $(70 \times 70) \text{ \AA}^2$ , respectively. The unit cell is shown in each image as a dashed square. The molecule orientation is shown in the simulated positive-bias STM image.

V with the experimental ones taken at RT for the same bias voltages. In the experiment, the change of polarity produces an observable change in the shape of the molecular images. It can be seen that while at –1.6 V the molecules appear as ellipsoids elongated along the [100] directions, at +1.6 V the molecular images are approximately circular. These experimental images are part of a wider study of the bias-voltage dependence of the molecular image, which covered the range between –2 and +2 V. We found ellipsoidal shapes from –2 to +0.5 V, approximately, while circular spots were clearly observed above +1.5 V. The simulated images shown in Figure 9 reproduce the observed effect qualitatively. In the simulations, the molecules are imaged as spots with the brighter zone in the position of the C rings.

In order to understand the behavior of the STM images with the bias voltage, we analyzed the total and projected density of states (PDOS) of this phase. Figure 10 shows the total DOS calculated for the relaxed structure of the phase in a region of  $\pm 3$  eV around the Fermi level and also the projections of the DOS on the benzene ring (atoms labeled C1 and C2), on the C atoms of the carboxyl groups (labeled C3), and on the oxygen atoms. The PDOS related to the benzene ring dominates the total density of states above the Fermi level. In particular, it is responsible for the two features at 0.0–0.7 and 1.8–3.2 eV. On

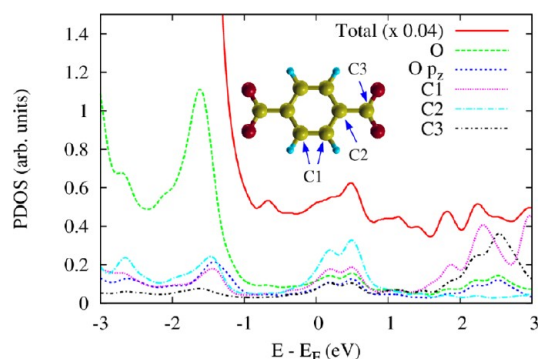


**Figure 10.** Calculated projected density of states (PDOS) corresponding to the ( $3 \times 3$ ) phase of deprotonated TPA molecules on the Cu(001) surface.

the other hand, the DOS corresponding to the filled states is dominated by the PDOS associated with O atoms. The main features appear below 1 eV, where the Cu d band begins, and a clear hybridization with O orbitals can be seen in the figure. The relatively small contribution of O  $p_z$  orbitals means that although the O atoms are close to a top position, the main hybridization comes from  $p_x$  and  $p_y$  orbitals pointing to the corresponding neighbor Cu atom. Although the O atoms have a high contribution for energies up to –1.6 eV, the difference in height with respect to the benzene ring (0.26 Å) makes them less visible in the STM images. The change in the spot shape of the STM images for positive and negative bias, can be understood by taking into account the difference in height between the C atoms in the ring ( $z_{C1} - z_{C2} = 0.1 \text{ \AA}$ ) and their corresponding PDOS (Figure 10). In fact, for negative bias both ring atoms have approximately the same PDOS, making the C2 atoms less visible in the STM image due to their lower height. On the other hand, for positive bias C2 atoms have a higher contribution in the PDOS that compensates for their lower height and they become more visible, resulting in the squarelike shape in the STM images.

Therefore, by comparing the experimental and simulated images, we can conclude that the spots in the negative bias STM images are elongated perpendicular to the long molecular axis.

For the molecular configuration in the  $9\sqrt{2}$  phase, the high-resolution STM image shown in the upper part of Figure 11, as well as the one in Figure 4b of Stepanow et al.,<sup>12</sup> suggest that the molecules are adsorbed with the long axis parallel to the [110] and  $[\bar{1}10]$  directions. Since our HR-XPS data indicate that this phase contains both complete and deprotonated carboxyl groups, we have performed DFT calculations for possible configurations with different degrees of deprotonation. Moreover, we also considered the possible formation of structures with Cu adatoms, already observed by Wang et al.<sup>37</sup> for TPA adsorption on Cu(110).

In Figure 12 we show the four relaxed configurations that have the highest adsorption energy, out of eight considered configurations. The two calculated relaxed structures with adsorbed Cu atoms are not shown, as they have lower molecule adsorption energy by more than 0.20 eV. In this figure, configuration a corresponds to semideprotonated molecules as proposed by Stepanow et al.<sup>12</sup> but with a different arrangement of the OH groups of the molecules. Configuration b corresponds to totally deprotonated molecules, while c and d correspond to structures with half the molecules totally



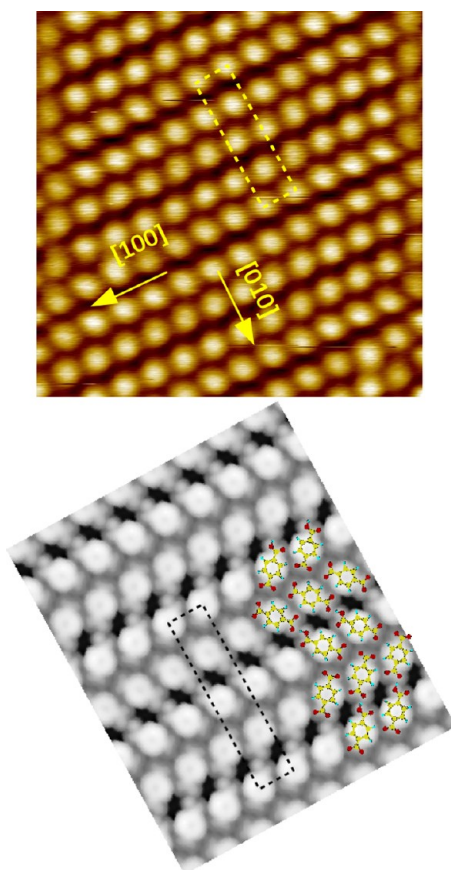


**Figure 11.** Experimental (top) and simulated (bottom) STM images for the  $9\sqrt{2}$  phase. The unit cell is shown as dashed rectangles in both STM images. The tunneling conditions are  $-2.0$  V/ $50$  pA, and the size corresponding to the experimental image is  $(100 \times 100)$  Å<sup>2</sup>.

		$E_{\text{ads}}(\text{eV})$
(a) 4 OH		1.75
(b) no OH		1.79
(c) 2 OH		1.81
(d) 2 OH		2.01

**Figure 12.** Relaxed configurations of different possible molecular geometries for the  $9\sqrt{2}$  phase, which are close in adsorption energy. For each configuration, we indicate on the left the number of OH groups, and on the right the corresponding adsorption energy per molecule in electronvolts.

deprotonated and the other half semideprotonated. Among the configurations analyzed, configuration d is the most stable one. This configuration has an adsorption energy of  $2.01$  eV/molecule which is lower than the values obtained for the deprotonated molecule, either isolated or in the  $(3 \times 3)$  phase, but higher than the value obtained for the complete adsorbed molecule. From the rather large difference ( $>0.20$  eV) in the adsorption energy for this molecular geometry compared to the other possible configurations, we conclude that this is the molecular configuration of the  $9\sqrt{2}$  phase.

As shown in detail in Figure 13, the  $9\sqrt{2}$  unit cell thus contains two RCOOH groups and six deprotonated groups

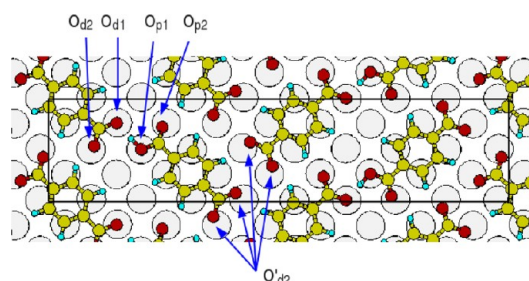


**Figure 13.** The  $(9\sqrt{2} \times 2\sqrt{2})$   $R45^\circ$  unit cell corresponding to the lowest-energy configuration.  $O_{p1}$  and  $O_{p2}$  are chemically inequivalent O atoms coming from the complete carboxyl groups, while  $O_{d1}$ ,  $O_{d2}$ , and  $O'_{d2}$  are chemically inequivalent O atoms coming from the carboxylates. See text for details.

(RCOO<sup>-</sup>), with the RCOOH groups facing the RCOO<sup>-</sup> ones. To simplify the analysis, we classify the 16 O atoms in four chemically inequivalent groups, two of them coming from the RCOOH groups (denoted by  $O_{p1}$  and  $O_{p2}$ ) and the other two coming from the deprotonated carboxyl ones ( $O_{d1}$  and  $O_{d2}$ ). Although  $O_{d1}$  atoms belong to deprotonated groups, they form H-bonds and we then expect some difference with respect to the rest of O atoms in RCOO<sup>-</sup> groups ( $O_{d2}$  atoms). For the relaxed structure, we calculated the distances of the O atoms to the Cu nearest neighbor, finding values of  $2.08$ ,  $2.23$ , and  $2.01$ – $2.06$  Å for  $O_{p2}$ ,  $O_{d1}$ , and  $O_{d2}$  atoms, respectively. We can see that the  $O_{d1}$  atoms are displaced upward significantly due to formation of the hydrogen bond.

In order to further elucidate the contributions of  $O_{p2}$  and  $O_{d1}$  atoms to the XPS O 1s spectrum (Figure 6), we calculated the relative shifts of O 1s levels of all O atoms in the unit cell. These relative core level shifts are calculated as total-energy differences of the same system containing a core hole at different positions.<sup>40</sup> In this way, the screening of the hole in the final state is taken into account. The core hole is described by means of a pseudopotential for O generated with a hole in the 1s level. Relative to the  $O_{p1}$  1s level, we obtain values of  $1.18$ ,  $1.35$ , and  $1.58$ – $1.69$  eV for  $O_{p2}$ ,  $O_{d1}$ , and  $O_{d2}$  1s levels, respectively. We note that the shift higher than  $0.2$  eV between the core levels of  $O_{d1}$  and  $O_{d2}$  atoms reflects the differences between the corresponding Cu–O bond lengths discussed above. In the inset of Figure 6, we show a simulated XPS spectrum that uses for each O peak a Gaussian function with a width of  $0.5$  eV. It reproduces qualitatively well the experimental O 1s core level spectrum of the  $9\sqrt{2}$  phase. Even when the calculated chemical shifts for  $O_{p2}$  and  $O_{d2}$  1s levels are systematically lower than the values expected for C=O and carboxylate groups relative to OH peak, we can expect an experimentally distinguishable shift of the  $O_{d1}$  peak



with respect to the peak positions of the O<sub>d2</sub> atoms. This effect might explain the shift of 1.6 eV and the higher intensity of component II with respect to component III.

Finally, from the relaxed structure of this configuration for the  $9\sqrt{2}$  phase (Figure 13), we simulated STM images for positive and negative bias voltage  $V_b$ . Figure 11 compares the simulation obtained for  $V_b = -2.0$  V with an experimental image taken at RT for the same bias voltages. In the simulated images, the spots corresponding to the semideprotonated molecules are brighter than the spots of the totally deprotonated molecules. This difference comes from the OH groups, which in the relaxed structure are higher from the surface than the C-ring. In the experimental images shown in Figure 11, there is no appreciable difference in brightness between lines of spots. However, several other images present this effect as we show in Figure 14. This image presents a region where we clearly see alternate lines with brighter spots, and the abrupt change in the top of this region points to an effect due to the STM tip.

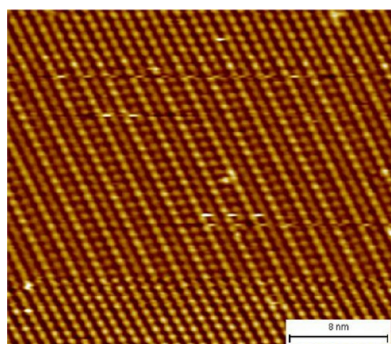


**Figure 14.** Experimental STM image of the  $9\sqrt{2}$  phase taken with a bias voltage of  $-2$  V and a tunneling current of  $10$  pA. This image illustrates how the appearance of the  $9\sqrt{2}$  phase can change due to tip effects.

## DISCUSSION

We show in Figure 15 a comparative scheme of the adsorption energy values obtained for the different phases analyzed

$\theta \rightarrow 0$	$\theta = 1/9$	$\theta = 1/8$
protonated — 1.80 eV	$9\sqrt{2} \times 2\sqrt{2}$ <div> — 1.75 eV  — 1.79 eV  — 1.81 eV  — 2.01 eV </div>	$2\sqrt{2} \times 4\sqrt{2}$ — 1.80 eV
deprotonated — 2.08 eV		
	$3 \times 3$ — 2.28 eV	

**Figure 15.** Summary of the adsorption energies theoretically obtained for the different phases and configurations considered in this work. van der Waals interactions were considered in the corresponding DFT calculations. See text for details.

theoretically in this work. The first column starting from the left shows the adsorption energies obtained for isolated molecules; the second one corresponds to the cases of  $9\sqrt{2}$  and the  $(3 \times 3)$  phases, both of them corresponding to a molecular coverage of 1 molecule per 9 Cu atoms of the first

surface layer ( $\theta = 1/9$ ). In the third column we include a phase that was obtained from the calculations for a molecular coverage of 1 molecule per 8 Cu atoms of the first surface layer ( $\theta = 1/8$ ). This phase corresponds to a  $(2\sqrt{2} \times 4\sqrt{2})$   $R45^\circ$  structure with two deprotonated TPA molecules in the unit cell, oriented as in the  $9\sqrt{2}$  phase but with a more compact arrangement, as can be seen in Figure 16. Remarkably, the  $c(3$

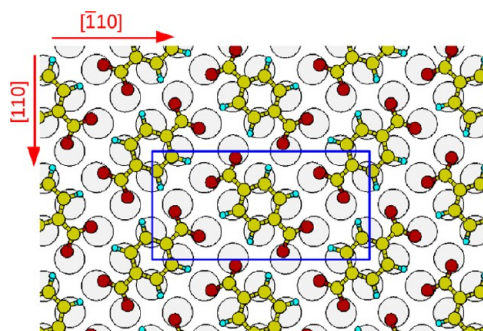


**Figure 16.** Molecular geometry for the calculated relaxed configuration of the  $(2\sqrt{2} \times 4\sqrt{2})$   $R45^\circ$  molecular structure.

$\times 5$ ) phase recently reported by Tait et al.<sup>35</sup> for the TPA/Cu(001) system most probably corresponds to the  $(2\sqrt{2} \times 4\sqrt{2})$   $R45^\circ$  structure found in this work. In addition, a similar structure has also been recently observed for TPA molecules adsorbed on Cu(110).<sup>37</sup> Although with the  $(2\sqrt{2} \times 4\sqrt{2})$   $R45^\circ$  structure there is no gain in adsorption energy with respect to isolated molecules, it corresponds to the lying-down phase with the highest possible molecule coverage.

**The  $(3 \times 3)$  Phase.** As expected from the experimental data, the  $(3 \times 3)$  phase is the most stable phase of the system, with an energy gain produced by the assembly of the phase of 0.20 eV/molecule (with respect to the isolated molecule). In this phase, the dominant molecule/substrate interaction comes from the formation of strong O—Cu bonds; it imposes a defined registry of the molecules with respect to the substrate. Specifically, the terephthalates are located with the center of the C ring on a hollow site of the surface and the O atoms at positions nearly atop Cu atoms of the first surface layer; this adsorption geometry is very similar to that obtained for isolated deprotonated molecules. In addition, the formation of Cu—O bonds produces a bending of the molecules and a corrugation of the first Cu layer. Interestingly, the six C atoms of the rings are no longer equivalent as a consequence of the bending, producing an observable effect in the STM images.

Two main intermolecular interactions can then be identified as responsible for the self-assembly of the  $(3 \times 3)$  phase: (i) formation of weak  $[C-H\cdots O]$  hydrogen bonds between the O atoms of a molecule and the H atoms of the aromatic ring of its nearest-neighbor molecules and (ii) surface-mediated interaction. Regarding the  $[C-H\cdots O]$  bonds, a wealth of structural data revealed that the distance between H and O atoms,  $d(H\cdots O)$ , is typically found in the range 2.0–3.0 Å.<sup>24</sup> In the calculated  $(3 \times 3)$  structure, the  $d(H\cdots O)$  distance is 2.17 Å and the angle is  $152.2^\circ$ . We note that while the distance is consistent with strong  $[C-H\cdots O]$  bonds, the angle is, in turn, quite far from the optimal one ( $180^\circ$ ).

On the other hand, it was recently shown that, in the case of 7,7,8,8-tetracyanoquinodimethane (TCNQ) molecules adsorbed on Cu(001) surfaces, the buckling of the first substrate layer induced by the strong bonds formed between the cyano

groups and the Cu atoms plays a determinant role in the molecular self-assembly.<sup>4</sup> In this case the increase of the surface elastic energy produced by the buckling is the driving force for a strong surface-mediated attractive intermolecular interaction that leads to the observed molecular islanding. Our calculations for an isolated deprotonated TPA molecule (see Figure 7) predict important vertical displacements ( $\sim 0.12$  Å) of the Cu atoms underneath the adsorbed molecule, and therefore, we can expect important surface-mediated intermolecular interactions also in the case of the  $(3 \times 3)$  phase. As mentioned in the Introduction, Ge et al.<sup>23</sup> reported that no evidence of [C–H...O] bonds was detected in their HREELS spectra of the  $(3 \times 3)$  phase, and hence, it was suggested that the TPA islanding may occur due to surface-mediated attractive interactions. Our theoretical results are consistent with the proposed hypothesis.

**The  $9\sqrt{2}$  Phase.** This phase presents peculiar characteristics. It contains [O–H...O] bonds that are not formed between the two RCOOH groups but between an OH and an O atom of a deprotonated carboxyl group. Interestingly, our calculations predict that the  $O_{d1}$  atom (see Figure 13) is displaced upward due to formation of the hydrogen bond, significantly reducing the interaction with the Cu atom beneath. In turn,  $O_{p2}$  atoms in the RCOOH groups get closer to their nearest-neighbor Cu atom, achieving a bond distance close to that found in the relaxed  $(3 \times 3)$  phase.

The obtained O–Cu distances for the relaxed structure reflect something that emerged from the theoretical analysis of the isolated molecules: despite the fact that the  $O_{p2}$  atoms belong to protonated carboxyl groups, the  $O_{p2}$ –Cu distance turned out to be practically the same as the  $O_{d2}$ –Cu one. Furthermore, they are close to the O–Cu distance (2.01 Å) obtained for the  $(3 \times 3)$  phase.

The case of the  $O_{d1}$  atoms is especially interesting because, being part of carboxylates, they form [OH...O] bonds. The fact that the Cu–O distance (2.23 Å) is in this case considerably larger than that obtained for the  $O_{d2}$  atoms (2.01–2.06 Å), implies that the strength of the [O–H...O] interaction is comparable to that of the Cu–O one. In general, our theoretical analysis predicts strong Cu–O bonds between the O atoms of carboxylates and the Cu atoms of the surface. This fact is clearly reflected in the case of isolated molecules, where two adsorption-energy minima were found for terephthalates corresponding to the two different orientations of the molecule; in both cases a considerable buckling of the first surface layer was obtained. Remarkably, the high strength of the [O–H...O] interaction is consistent with the fact that the values of the corresponding geometrical parameters practically coincide with those found in TPA crystals; that is, they are close to ideal values. Specifically, the calculated distance between the O atoms of the [O–H...O] bonds in the  $9\sqrt{2}$  structure is 2.57 Å, while the calculated O–H–O angle is  $177.9^\circ$ . On the other hand, the distance between O atoms in the TPA crystal was experimentally determined to be 2.61 Å.<sup>41</sup>

We note that although the optimal orientation both for isolated molecules (by 0.20 eV) and for the  $(3 \times 3)$  phase was determined to be the  $\langle 100 \rangle$  one, the four molecules in the  $9\sqrt{2}$  unit cell are oriented along the  $\langle 110 \rangle$  and equivalent directions. We can then conclude that the formed [O–H...O] bonds are able to compensate the energy cost of a more expensive azimuthal orientation. The network of [O–H...O] bonds thus plays an essential role in the stabilization of the  $9\sqrt{2}$  phase.

Finally, the strong interaction between the O atoms in carboxylates and the Cu atoms in the steps produces

reorientation of the steps along the  $\langle 100 \rangle$  directions. Notably, our STM images indicate that the molecules adsorb at the lower edge of the steps with their long axes oriented as in the  $9\sqrt{2}$  phase, that is, along  $\langle 110 \rangle$  directions. It is interesting to note that although the adsorption of the molecules at RT produces an important mass transport in the surface, neither the  $(3 \times 3)$  nor the  $9\sqrt{2}$  phase contains Cu adatoms in the structure.

## CONCLUSIONS

The main conclusions derived from this study are the following. Our theoretical results indicate the formation of strong bonds between the O atoms in carboxylates and the Cu atoms of the surface, which causes a bending of the molecules and a buckling of the first Cu layer. In the  $(3 \times 3)$  phases, it was shown that the bending produces observable effects in the molecular STM images. It was also observed that the strong interaction between the carboxylates and the Cu atoms at the step edges causes reorientation of the surface steps along the  $\langle 100 \rangle$  crystallographic directions.

Regarding the metastable  $\beta$  phase, it was experimentally determined that it has a  $(9\sqrt{2} \times 2\sqrt{2})$   $R45^\circ$  unit cell and exactly the same molecular coverage as the  $(3 \times 3)$  phase (1 TPA molecule per 9 Cu atoms in the first surface layer). When TPA molecules are deposited on the Cu(001) sample kept at RT, most of them adopt the  $(9\sqrt{2} \times 2\sqrt{2})$   $R45^\circ$  structure; this situation was found to be stable for several hours. The lowest-energy structure theoretically found for the  $(9\sqrt{2} \times 2\sqrt{2})$   $R45^\circ$  phase contains two totally deprotonated molecules and two semideprotonated molecules in the unit cell (see Figure 13). In this molecular structure the [O–H...O] bonds are formed between an OH group and an O atom of a deprotonated carboxyl group. This network of [O–H...O] bonds plays a fundamental role in the stabilization of the structure.

With respect to the irreversible  $9\sqrt{2} \rightarrow (3 \times 3)$  transition, the results reported in this work conclusively show that it involves the following two processes: (i) deprotonation of neutral carboxyl groups remaining in the metastable phase and (ii) rearrangement of molecules into the  $3 \times 3$  configuration.

## AUTHOR INFORMATION

### Corresponding Author

\*E-mail fuhr@cab.cnea.gov.ar (J.D.F.), ascolani@cab.cnea.gov.ar (H.A.).

### Notes

The authors declare no competing financial interest.

## ACKNOWLEDGMENTS

We thank Dr. Magalí Lingenfelder for helpful discussions. We acknowledge financial support by the following Argentine institutions: CONICET (PIP 112 200801 00958), J.A. Balseiro and ANTORCHAS foundations, and ANPCYT (PICT2005/33432, PME 2003/118), UNCuyo (Grants 06/C390). We also acknowledge financial support from the ICTP-Elettra Users Programme. We also thank CONICET for the fellowships of N.M.-Q. and L.C. Three of us (J.D.F., J.E.G., and H.A.) are members of CONICET of Argentina.

## REFERENCES

- (1) Barth, J. V.; Costantini, G.; Kern, K. *Nature* **2005**, *437*, 671–679.
- (2) Barth, J. V. *Annu. Rev. Phys. Chem.* **2007**, *58*, 375–497.

- (3) Elemans, J. A. A. W.; Lei, S.; de Feyter, S. *Angew. Chem., Int. Ed.* **2009**, *48*, 7298–7332.
- (4) Tseng, T.-C.; Urban, C.; Wang, Y.; Otero, R.; Tait, S. L.; Alcamí, M.; Écija, D.; Trelka, M.; Gallego, J. M.; Lin, N.; et al. *Nat. Chem.* **2010**, *2*, 374–379.
- (5) Stepanow, S.; Ohmann, R.; Leroy, F.; Lin, N.; Strunskus, T.; Wo, C.; Kern, K. *ACS Nano* **2010**, *4*, 1813–1820.
- (6) Clair, S.; Pons, S.; Seitsonen, A. P.; Brune, H.; Kern, K.; Barth, J. *J. Phys. Chem. B* **2004**, *108*, 14585–14590.
- (7) Ye, Y.; Sun, W.; Wang, Y.; Shao, X.; Xu, X.; Cheng, F.; Li, J.; Wu, K. *J. Phys. Chem. C* **2007**, *111*, 10138–10141.
- (8) Zhou, H.; Dang, H.; Yi, J.-H.; Nanci, A.; Rochefort, A.; Wuest, J. D. *J. Am. Chem. Soc.* **2007**, *129*, 13774–13775.
- (9) Dubois, L.; Zegarski, B.; Nuzzo, R. *Langmuir* **1986**, *2*, 412–417.
- (10) Chen, Q.; Perry, C. C.; Frederick, B. G.; Murray, P. W.; Haq, S.; Richardson, N. V. *Surf. Sci.* **2000**, *446*, 63–75.
- (11) Messina, P.; Dimitriev, A.; Lin, N.; Spillmann, H.; Abel, M.; Barth, J. V.; Kern, K. *J. Am. Chem. Soc.* **2002**, *124*, 14000–14001.
- (12) Stepanow, S.; Strunskus, T.; Lingenfelder, M.; Dimitriev, A.; Spillmann, H.; Lin, N.; Barth, J.; Wöll, C.; Kern, K. *J. Phys. Chem. B* **2004**, *108*, 19392–19397.
- (13) Classen, T.; Lingenfelder, M.; Wang, Y.; Chopra, R.; Virojanadara, C.; Starke, U.; Contantini, G.; Fratesi, G.; Fabris, S.; de Gironcoli, S.; et al. *J. Phys. Chem. A* **2007**, *111*, 12589–12603.
- (14) Faraggi, M.; Rogero, C.; Arnau, A.; Trelka, M.; Ecija, D.; Isvoranu, C.; Schnadt, J.; Mart-Gastaldo, C.; Coronado, E.; Gallego, J.; et al. *J. Phys. Chem. C* **2011**, *115*, 21177–21182.
- (15) Parker, B.; Immaraporn, B.; Gellman, A. J. *Langmuir* **2001**, *17*, 6638–6646.
- (16) Schnadt, J.; Rauls, E.; Xu, W.; Vang, R.; Knudsen, J.; Lægsgaard, E.; Li, Z.; Hammer, B.; Besenbacher, F. *Phys. Rev. Lett.* **2008**, *100*, No. 046103.
- (17) Spillmann, H.; Dimitriev, A.; Nian, L. N.; Messina, P.; Barth, J. V.; Kern, K. *J. Am. Chem. Soc.* **2003**, *125*, 10725–10728.
- (18) Lingenfelder, M.; Spillmann, H.; Dimitriev, A.; Stepanow, S.; Lin, N.; Barth, J. V.; Kern, K. *Chem.—Eur. J.* **2004**, *10*, 1913–1919.
- (19) Tait, S.; Wang, Y.; Costantini, G.; Lin, N.; Baraldi, A.; Esch, F.; Petaccia, L.; Lizzit, S.; Kern, K. *J. Am. Chem. Soc.* **2008**, *130*, 2108–2110.
- (20) Wang, Y.; Fabris, S.; Costantini, G.; Kern, K. *J. Phys. Chem. C* **2010**, *114*, 13020–13020.
- (21) Gambardella, P.; Stepanow, S.; Dimitriev, A.; Honolka, J.; de Groot, F. M. F.; Lingenfelder, M.; Gupta, S.; Sarma, D. D.; Bencok, P.; Stanesco, S.; et al. *Nat. Mater.* **2009**, *8*, 189–193.
- (22) Tseng, T.-C.; Lin, C.; Shi, X.; Tait, S. L.; Liu, X.; Starke, U.; Lin, N.; Zhang, R.; Minot, C.; Hove, M. A. V.; et al. *Phys. Rev. B* **2009**, *80*, No. 155458.
- (23) Ge, Y.; Adler, H.; Theertham, A.; Kesmodel, L. L.; Tait, S. L. *Langmuir* **2010**, *26*, 16325–16329.
- (24) Desiraju, G. R. *Acc. Chem. Res.* **1996**, *29*, 441–449.
- (25) Gotter, R.; Ruocco, A.; Morgante, A.; Cvetko, D.; Floreano, L.; Tommasini, F.; Stefani, G. *Nucl. Instrum. Methods Phys. Res. A* **2001**, *467*, 1468–1472.
- (26) Floreano, L.; Naletto, G.; Cvetko, D.; Gotter, R.; Malvezzi, M.; Marassi, L.; Morgante, A.; Santaniello, A.; Verdini, A.; Tommasini, F.; et al. *Rev. Sci. Instrum.* **1999**, *70*, 3855–3865.
- (27) Cautero, G.; Sergio, R.; Stebel, L.; Lacovig, P.; Pittana, P.; Pedronzani, M.; Carrato, S. *Nucl. Instrum. Methods Phys. Res. A* **2008**, *595*, 447–459.
- (28) Giannozzi, P.; Baroni, S.; Bonini, N.; Calandra, M.; Car, R.; Cavazzoni, C.; Ceresoli, D.; Chiarotti, G. L.; Cococcioni, M.; Dabo, I.; et al. *J. Phys.: Condens. Matter* **2009**, *21*, No. 395502.
- (29) Lee, K.; Murray, É. D.; Kong, L.; Lundqvist, B. I.; Langreth, D. C. *Phys. Rev. B* **2010**, *82*, No. 081101.
- (30) Cooper, V. R. *Phys. Rev. B* **2010**, *81*, No. 161104.
- (31) Bengtsson, L. *Phys. Rev. B* **1999**, *59*, 12301–12304.
- (32) Tersoff, J.; Hamann, D. R. *Phys. Rev. B* **1985**, *31*, 805–813.
- (33) We used the LEEDpat 3.0 software by K. Hermann and M. A. Van Hove.
- (34) Katayama, T.; Mukai, K.; Yoshimoto, S.; Yoshinobu, J. *Phys. Rev. B* **2011**, *83*, No. 153403.
- (35) Tait, S.; Lim, H.; Theertham, A.; Seidel, P. *Phys. Chem. Chem. Phys.* **2012**, *14*, 8217–8223.
- (36) Giessen-Seibert, M.; Jentjens, R.; Poensgen, M.; Ibach, H. *Phys. Rev. Lett.* **1993**, *71*, 3521–3524.
- (37) Wang, Y.; Fabris, S.; White, T.; Pagliuca, F.; Moras, P.; Topwal, M. P. D.; Sheverdyayeva, P.; Carbone, C.; Lingenfelder, M.; Classen, T.; et al. *Chem. Commun.* **2012**, *48*, 534–536.
- (38) McQuaide, B. H.; Banna, M. S. *Can. J. Chem.* **1988**, *66*, 1919–1922.
- (39) Cossaro, A.; Puppini, M.; Cvetko, D.; Kladnik, G.; Verdini, A.; Coreno, M.; de Simone, M.; Floreano, L.; Morgante, A. *J. Phys. Chem. Lett.* **2011**, *2*, 3124–3129.
- (40) Pehlke, E.; Scheffler, M. *Phys. Rev. Lett.* **1993**, *71*, 2338–2341.
- (41) Bailey, M.; Brown, C. J. *Acta Crystallogr.* **1967**, *22*, 387–391.